We thank both reviewers for their careful reading of our paper and their very valuable comments. We repeat the reviewer comments below in italics, then give our responses.

Reviewer 1, Comment 1

Reviewer comment

1 The rationale for selecting Shanghai and Lishui as representative urban and rural environments within the YRD requires stronger justification. The conclusions are largely based on two locations, yet the manuscript frequently discusses implications for the broader YRD region. While case studies are useful for mechanistic analysis, the limited spatial sampling raises concerns regarding regional representativeness. Given the dense air-quality monitoring network across the YRD, the authors should explain why a broader regional classification was not conducted and discuss the extent to which the selected sites capture the diversity of chemical regimes across the region.

Response

In the revised manuscript, we have substantially strengthened the justification for selecting Shanghai and Lishui and clarified the intended extent of their representativeness. Specifically, we have added a YRD-wide comparison based on 250 AQMS sites, the 2018 Global Urban Boundary dataset and observed JJA 2022 NO_2 concentrations in the revised Fig. 1 and Sect. 2.1 (lines 130-161). We now distinguish explicitly between the populated urban/suburban locations sampled by the Lishui AQMSs and the broader lower-NO_x, biogenically influenced regional environment represented by the box model (Table 1; lines 150-184). Finally, Fig. 6 independently diagnoses the contrasting VOC-limited and NO_x-limited chemical regimes represented by Shanghai and Lishui (lines 470-500).

Shanghai and Lishui were deliberately selected as two contrasting chemical environments within the YRD. Shanghai represents a densely urbanised megacity environment with strong anthropogenic precursor influence, whereas Lishui represents a substantially lower-NO_x environment with stronger influence from surrounding vegetation (lines 138-141). This contrast is central to the experimental design because the study aims to determine how the O_3 response to temperature changes between different precursor-sensitivity regimes.

(a)

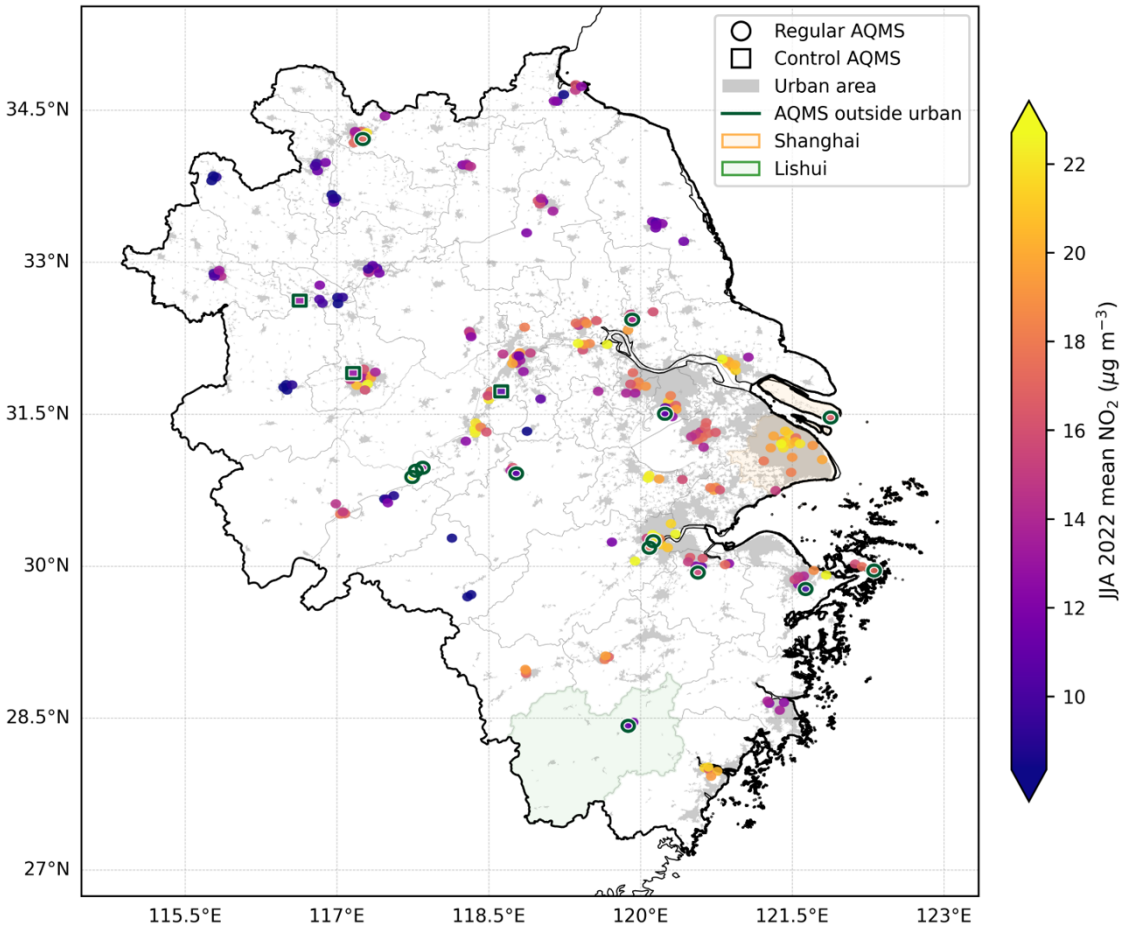

(b) YRD site-level NO_2 distribution and selected-site position

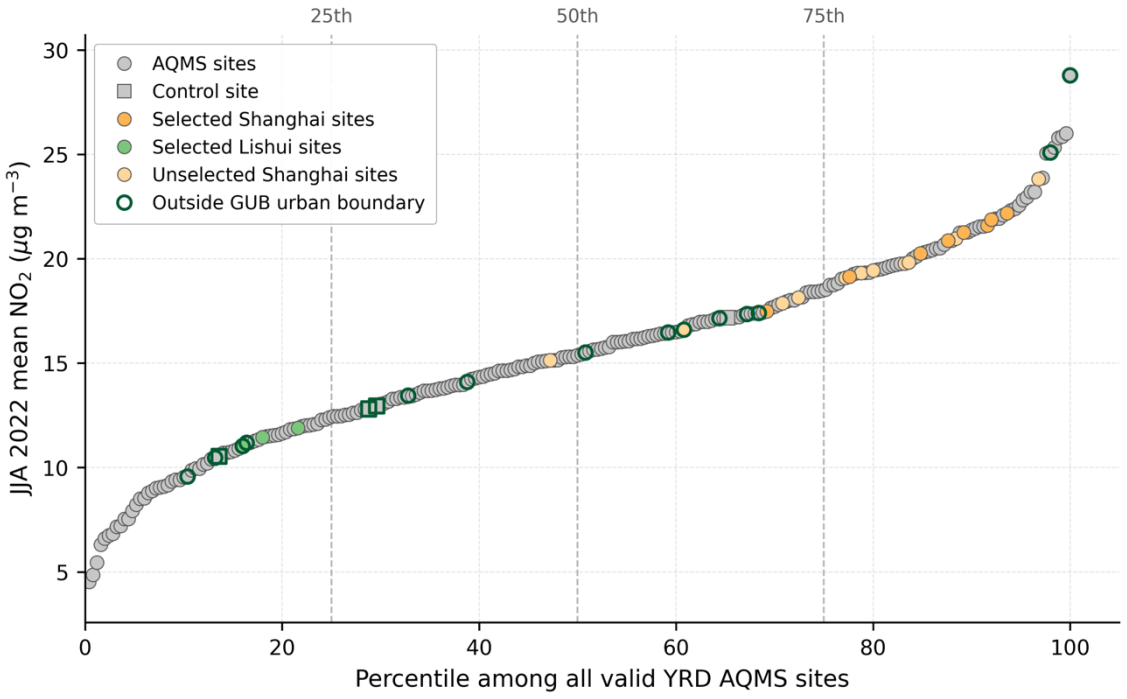

Figure 1. (a) Spatial distribution of Air Quality Monitoring Sites (AQMS) across the YRD in summer 2022, coloured by JJA 2022 mean NO_2. Grey shading indicates the 2018 Global Urban Boundaries (GUB) urban settlement extent. Circular markers denote regular AQMS, square markers denote control sites, and green outlines indicate sites located outside the GUB urban settlement boundary. Shanghai and Lishui are highlighted by coloured city polygons. (b) Ranked distribution of JJA 2022 mean NO_2 across all valid YRD AQMS, expressed as site percentile. Selected Shanghai and Lishui sites (listed in Table 1) are highlighted in orange and green, respectively; unselected Shanghai sites are shown in pale orange, and sites outside the GUB urban boundary are outlined in dark green. Administrative boundaries from the GADM database (www.gadm.org).

To place this selection within the wider regional context, we expanded the analysis to include all 250 YRD AQMS sites satisfying the JJA 2022 data-validity criterion. The revised Figure 1 (see above) shows the spatial distribution of these sites relative to mapped urban-settlement boundaries and colours each site by its observed JJA mean NO_2 concentration (lines 130-151). This provides a consistent regional indicator of anthropogenic precursor influence.

The results demonstrate a clear separation between the selected environments. All eight Shanghai AQMSs are situated within mapped urban-settlement polygons and have a mean JJA NO_2 concentration of 20.58 μg m^{-3}, corresponding to approximately the 87th percentile of the 250-site YRD distribution (lines 148-151). By contrast, the three Lishui AQMSs have a mean NO_2 concentration of 11.46 μg m^{-3}, corresponding to approximately the 18th percentile (lines 152-156). Shanghai and Lishui therefore occupy clearly separated positions within the observed YRD precursor distribution: Shanghai represents the densely urbanised, high-NO_2 end, while Lishui represents a much lower-NO_2 regional environment. These results demonstrate objectively that the selected locations are not arbitrary outliers.

The regional land-surface and population characteristics provide an independent line of evidence. The Shanghai region (pale orange shading in Figure 1a) has a population density of approximately 3900 km^{-2}, and construction land covers 42.4 % of its area. Lishui (pale green shading in Figure 1a) has a population density of approximately 140 km^{-2}, 81.7 % forest cover, and an urban district accounting for approximately 8.6 % of its total area (lines 158-161). The two areas therefore differ substantially in urbanisation and vegetation influence, consistently reinforcing the contrast established by the regional NO_2 analysis.

The dense YRD monitoring network does not provide equivalent coverage of all environmental classes because routine AQMS are concentrated predominantly in populated urban settlements, as shown in the revised Figure 1 (lines 130-136). The Lishui AQMSs are consequently classified explicitly as urban/suburban locations in the revised Table 1. However, these receptors are embedded within a much less urbanised, lower-NO_x and more vegetation-influenced regional setting. The revised manuscript now distinguishes clearly between the immediate monitoring environment and the broader regional chemical environment represented by the Lishui box-model configuration (lines 180-184). This distinction allows the observations to be interpreted accurately while retaining the strong Shanghai-Lishui chemical contrast required by the study.

The availability of published isoprene measurements also supports the selection of these environments. These measurements provide direct observational references for the urban Shanghai and forest-influenced Lishui BVOC environments, which is particularly important because temperature-dependent isoprene emissions are examined explicitly in the box-model

experiments. The corresponding observational and simulated C_5H_8 concentrations are reported in Table 4 and discussed at lines 505-510. Isoprene measurements are not readily available for other sites.

The two locations also share the broader YRD summer climate setting and were analysed over the same severe regional heatwave period in JJA 2022 (lines 138-141 and 167-170). This provides a coherent climatic basis for comparison while retaining the strong differences in precursor abundance, urbanisation, vegetation influence and chemical regime. The purpose of the site selection is therefore to examine chemical-regime dependence within a common regional and seasonal setting, rather than to compare two unrelated climatic regions.

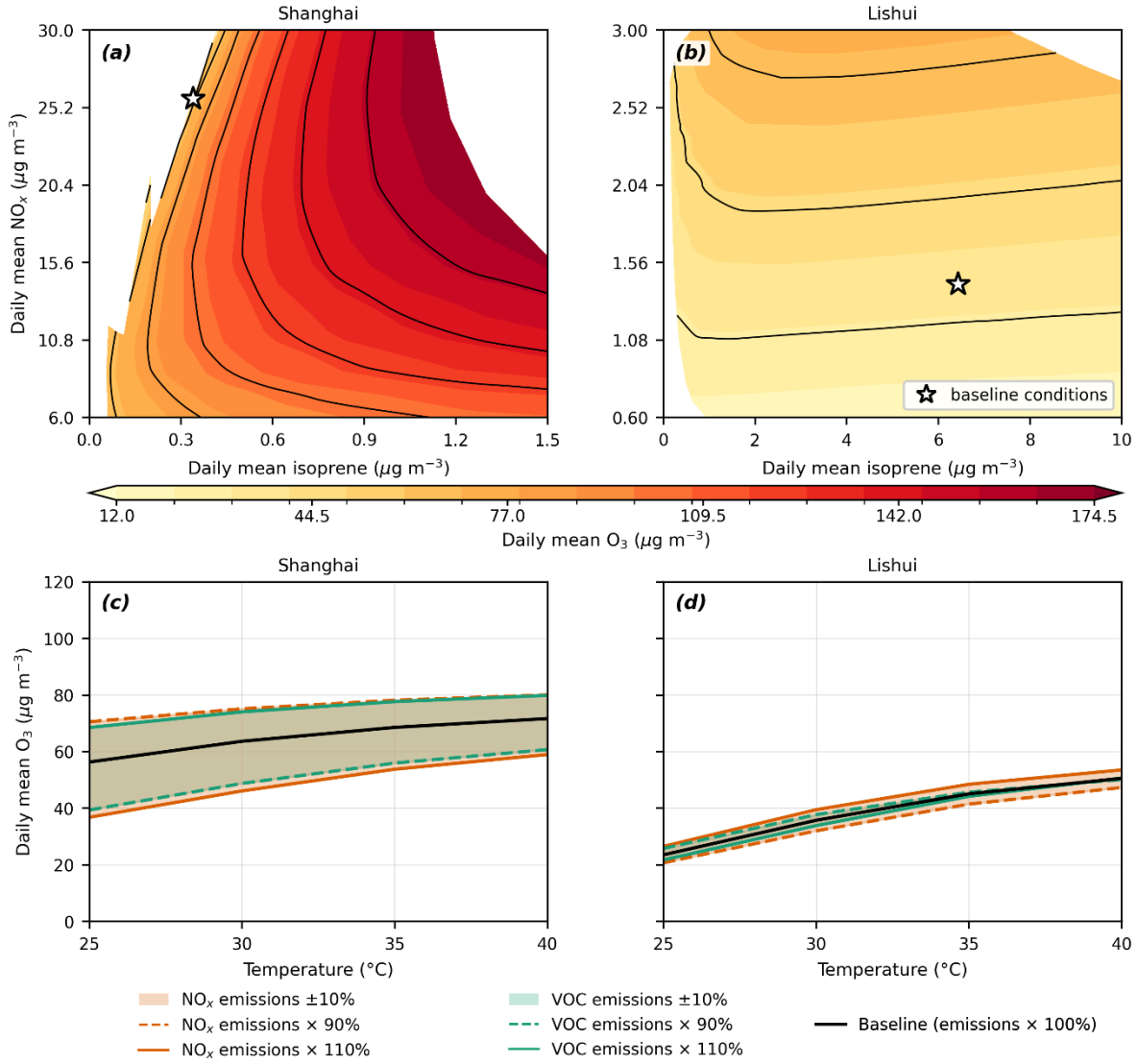

Figure 6. Simulated precursor sensitivity of daily mean surface O_3 in Shanghai and Lishui using the UKCA Box Model under the VRH_Ori baseline configuration with emission changes. Panels (a) and (b) show box model simulations of the evolution of ozone as a function of NO_x (NO + NO_2) and isoprene at 30 °C. Colours indicate daily mean O_3, black lines denote O_3 contours, and white stars mark the baseline conditions. Panels (c) and (d)

show the temperature dependence of O_3 under ±10 % perturbations in NO_x and VOC emissions at 25, 30, 35, and 40 °C.

Finally, the newly added O_3-NO_x-isoprene response surfaces provide a direct mechanistic diagnosis of the chemical environments represented by the two cases in the model. The Shanghai baseline lies within a VOC-limited regime, where O_3 increases with isoprene and decreases with increasing NO_x. In contrast, the Lishui baseline lies within a NO_x-limited regime, where O_3 responds positively to NO_x and only weakly to additional isoprene (Fig. 6a-b; lines 484-488). The ±10 % precursor perturbations confirm that these contrasting responses persist throughout the investigated temperature range of 25-40 °C (Fig. 6c-d; lines 489-500).

Taken together, the YRD-wide AQMS analysis, urban-settlement distribution, NO_2 percentiles, land-surface characteristics, available isoprene observations and precursor-response surfaces provide mutually consistent evidence for the site selection. Shanghai and Lishui capture a major and mechanistically important dimension of chemical diversity across the YRD: a high-NO_x, VOC-limited urban megacity environment and a lower-NO_x, NO_x-limited, vegetation-influenced regional environment.

Reviewer 1, Comment 2

Reviewer comment

2 The analysis is based exclusively on observations from 2022, an exceptionally hot summer characterized by severe heatwave conditions. Notably, the observed decrease in ozone sensitivity to temperature in Shanghai during heatwaves is an interesting result and appears consistent with recent studies reporting ozone suppression under extremely high temperatures. However, as acknowledged by the authors, conclusions derived from a single anomalous year may not be representative of climatological behavior. Extending the observational analysis to additional years would substantially improve the robustness of the conclusions and help determine whether the reported ozone-temperature relationships are specific to 2022 or representative of longer-term conditions. If possible, additional box-model simulations for other years should also be provided.

Response

In the revised manuscript, we have clarified why JJA 2022 was selected and how the observational and box-model results should be interpreted. Sect. 2.1 identifies 2022 as a severe, well-observed heatwave case and explains why the earlier major YRD heatwave summers of 2003 and 2013 could not provide the same continuous routine O_3 record (lines 167-170). Sect. 2.2.1 states that the 2022 observations and emissions define the baseline chemical environments, after which temperatures of 25-40 °C are imposed in controlled process-sensitivity experiments rather than used to reproduce the climatology of 2022 or any other year (lines 305-308). Sect. 3.1 reports the statistical interpretation of the Shanghai heatwave relationship (lines 410-418), and the Conclusions distinguish the 2022-specific numerical sensitivities from the broader process-level mechanisms (lines 893-902).

Summer 2022 was selected because it provides the combination required for this study: severe and persistent high-temperature conditions across the YRD together with continuous routine surface O_3 observations from the national monitoring network. Earlier major heatwave summers in the region, particularly 2003 and 2013, predate the availability of continuous O_3 observations. The 2022 event therefore provides a uniquely suitable recent case for connecting an observed O_3-temperature relationship with controlled chemical sensitivity experiments, as now explained at lines 167-170.

The observational component is consequently an extreme-event case study, not an estimate of the climatological mean O_3-temperature relationship. Its purpose is to characterise how O_3behaved across a wide temperature range during a severe and well-observed summer in two contrasting chemical environments. The manuscript now states this scope directly rather than treating the 2022 regressions as climatological sensitivities (lines 167-170 and 893-902).

We have also clarified the interpretation of the Shanghai heatwave result. The observed heatwave-period O_3-temperature slope remains positive at 3.49 μg m^{-3} $°C^{-1}$, but its 95 % confidence interval includes zero and the relationship is not statistically significant (95 % CI: −1.464 to 8.441 μg m^{-3} $°C^{-1}$; $p = 0.16$; $n = 41$). The result therefore demonstrates a loss of a statistically significant positive linear association during the 2022 Shanghai heatwaves, rather than a statistically established decrease or suppression of O_3 at extreme temperatures. By contrast, the heatwave relationship remains significantly positive in Lishui. These results and their statistical interpretation are reported at lines 410-418.

The box-model component has a different and complementary purpose. The UKCA Box simulations do not reproduce the meteorological history or climatological conditions of a particular year. The observations and emissions from 2022 are used to construct fixed Shanghai-like and Lishui-like baseline chemical environments. Temperature is then imposed independently from 25 to 40 °C, while the relevant chemical and environmental settings are controlled systematically. The simulations therefore determine how the same baseline chemical environment responds to temperature and allow the effects of chemical kinetics, humidity, diurnal thermal structure and temperature-dependent isoprene emissions to be separated (lines 305-308 and Sect. 2.3).

For this reason, repeating the box-model experiments under another nominal year would not constitute an independent simulation of that year's climate. The present experiment instead addresses the specific mechanistic question posed in this study: how temperature changes O_3 under fixed, contrasting Shanghai and Lishui chemical environments. The factorial design provides that diagnosis directly and avoids conflating temperature effects with interannual changes in emissions and background composition.

The study therefore combines two complementary forms of evidence. The observations document the O_3-temperature behaviour during the exceptional summer of 2022, while the controlled box-model experiments identify the chemical and emission-related mechanisms under fixed Shanghai-like and Lishui-like baseline environments. The mechanistic conclusions are supported independently by the temperature experiments, precursor-sensitivity diagnostics, and O_x, PAN and HO_x budget analyses. Adding further observational years would define additional precursor and background-chemical environments, but it would not add meteorological processes to the 0-D framework or turn the controlled temperature experiment into a climatological simulation.

We have revised the Conclusions accordingly. The quantitative observational slopes and model attribution fractions are identified as specific to the 2022 YRD emissions-meteorology setting and the controlled 0-D framework. At the same time, the diagnosed mechanisms: temperature-enhanced BVOC reactivity under VOC-limited urban conditions, radical-NO_x and PAN-mediated cycling under lower-NO_x conditions, and humidity modulation of O_x chemistry, are supported by the process diagnostics and are relevant to comparable chemical regimes (lines 893-902). This revised framing preserves the value of 2022 as a well-observed extreme-heat case while preventing the numerical results from being interpreted as a climatological projection.

Reviewer 1, Comment 3

Reviewer comment

3 Section 2.2 interweaves descriptions of the UKESM simulations and the UKCA box model, which confuses the overall modeling framework. I recommend separating this section into dedicated subsections, first describing the UKESM configuration and then the box-model setup. This will greatly improve readability.

Response

In the revised manuscript, we have reorganised the modelling Methods so that the two modelling frameworks and their distinct scientific roles are now described separately. Specifically, Sect. 2.2.1 now provides a self-contained description of the UKCA Box model configuration (lines 208-308), Sect. 2.2.2 separately describes the UKESM-AMIP configuration (lines 309-330), and Sect. 2.3 presents the box-model sensitivity experiments independently from both model descriptions (from line 332; Table 3).

We have placed the UKCA Box model subsection first because it is the primary process-attribution framework used in this study. This subsection now describes the zero-dimensional model structure, the shared StratTrop chemical mechanism, the prescribed meteorological conditions, the construction of the Shanghai-like and Lishui-like baseline chemical environments, and the emission and deposition inputs without interruption from UKESM configuration details (lines 208-308). It also explains that the box model is used to isolate controlled responses to temperature, humidity, diurnal temperature structure and temperature-dependent isoprene emissions (lines 209-231).

The UKESM-AMIP simulation is then described independently in Sect. 2.2.2. This subsection now contains the three-dimensional model resolution, chemistry and aerosol schemes, emission inventories, ERA5 nudging, simulation period, spin-up and output selection in one continuous description (lines 309-330). The revised structure makes clear that UKESM-AMIP provides supporting three-dimensional, same-chemistry context for selected O_x production and loss comparisons, whereas the UKCA Box model performs the controlled process experiments.

Finally, the experimental design has been moved into the separate Sect. 2.3, where Table 3 defines the factorial combinations of humidity treatment, diurnal temperature variation and temperature-dependent isoprene emissions. This organisation follows the scientific workflow of the study: the primary UKCA Box framework is introduced first, the supporting UKESM-AMIP configuration is defined second, and the controlled sensitivity experiments are then presented separately.

The revised structure therefore removes the previous interweaving of the two model descriptions and makes their complementary but distinct functions explicit.

Reviewer 1, Comment 4

Reviewer comment

4 The conclusion that BVOCs account for 73% of the ozone increase between 30 and 40 °C relies heavily on the parameterization used for temperature-dependent isoprene emissions. The authors should provide a stronger justification for adopting the simplified empirical function rather than the original MEGAN formulation and discuss the associated uncertainty. In addition, no local observational constraints on isoprene concentrations or emissions are provided. Given the lack of direct measurements, the uncertainty associated with BVOC attribution may be substantial.

Furthermore, the authors should address the temperature dependence of anthropogenic VOCs. Treating anthropogenic VOC emissions as temperature-independent may lead to an overestimation of the BVOC contribution. The potential influence of this assumption should be discussed in greater detail.

Response

In the revised manuscript, we have substantially strengthened the treatment of both temperature-dependent BVOC and AVOC emissions. Specifically, we now define the JULES/iBVOC temperature function and its 38.3 °C upper threshold explicitly in Sect. 2.3 and Fig. 3 (lines 335-359); compare the adopted JULES formulation directly with MEGAN v2.1, including the resulting isoprene and O_3 responses, in the new Sect. 4.2 (lines 799-825); include published C_5H_8 concentration constraints for both Shanghai and Lishui in Table 4 and the accompanying discussion (lines 501-510); quantify the potential temperature response of selected volatile chemical products (VCPs, also known as solvent use) related and gasoline-evaporation AVOC emissions in the new Sect. 4.1 (lines 770-797); and state explicitly in the Conclusions that the numerical BVOC fraction is conditional on the adopted isoprene-temperature parameterisation and Shanghai baseline emission setting (lines 846-856).

The isoprene emissions temperature-dependent function used in the main experiments was not introduced as an arbitrary empirical amplification. It is the JULES/iBVOC short-term temperature-response formulation used within the parent UKESM modelling framework (Pacifico et al., 2011). Adopting this formulation therefore maintains consistency between the UKCA Box experiments and the Earth System Model from which their land-surface and chemical framework is derived. The function is normalised to the prescribed 30 °C baseline and is defined as ($fT=\min[\exp(0.1(T-303.15)), 2.3]$). It increases exponentially until reaching its upper limit of 2.3 at 38.3 °C and remains constant thereafter (Fig. 3; lines 335-359).

To determine whether this simplified treatment produces an unrealistically strong high-temperature response, we directly compared it with the temperature activity factor implemented in MEGAN v2.1. MEGAN accounts for instantaneous temperature and thermal acclimation through the preceding 24 h and 240 h mean temperatures, rather than imposing a fixed upper threshold (Guenther et al., 2012). Both formulations were normalised to the same isoprene emission at 30 °C and applied over the same 30-40 °C experimental range (lines 799-813).

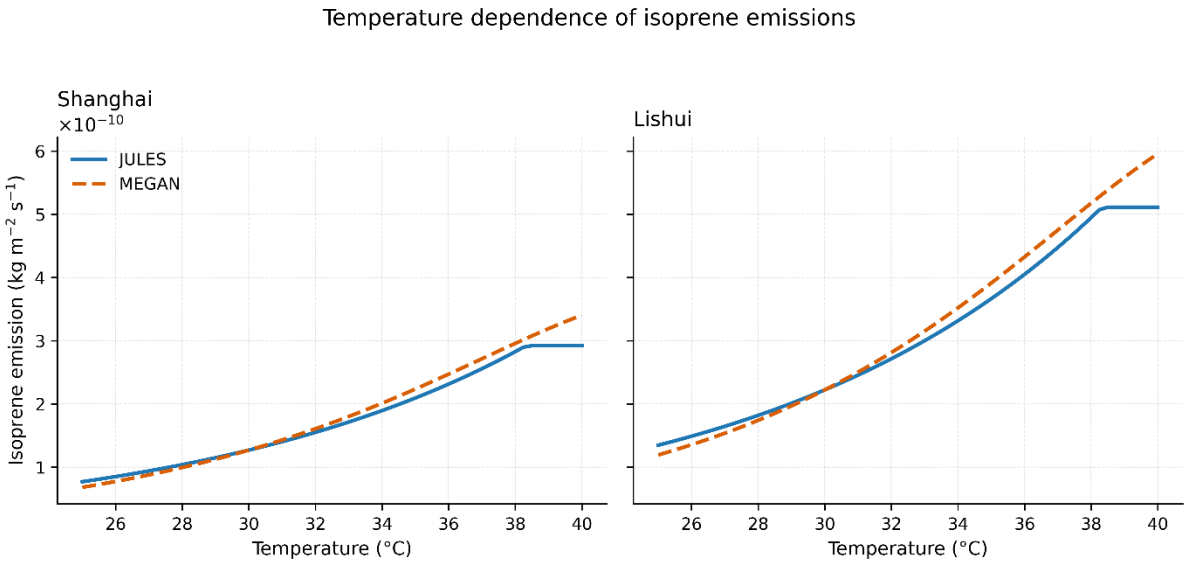

The comparison (see the figure above) demonstrates that the JULES formulation does not exaggerate the high-temperature isoprene response relative to MEGAN. At 40 °C, the JULES multiplier reaches 2.30, whereas the MEGAN multiplier reaches 2.68. The corresponding Shanghai isoprene fluxes are 2.92×10^{-10} and 3.40×10^{-10} kg m^{-2} s^{-1}, respectively, compared with their common 30 °C value of 1.27×10^{-10} kg m^{-2} s^{-1}. These represent increases of 130.0 % with JULES and 167.9 % with MEGAN (lines 810-816).

The resulting O_3 simulations lead to similar conclusions. Both schemes produce a daily maximum O_3 concentration of 116.1 μg m^{-3} at 30 °C. At 40 °C, O_3 reaches 202.1 μg m^{-3} using JULES and 215.5 μg m^{-3} using MEGAN, corresponding to 30-40 °C increases of 86.0 and 99.4 μg m^{-3}, respectively. MEGAN therefore produces 13.4 μg m^{-3} more O_3 than JULES at 40 °C. Both parameterisations independently support a large isoprene-driven amplification of urban O_3, while the fixed JULES cap produces the more conservative response near the upper end of the investigated temperature range (lines 818-825). This direct comparison confirms that the strong Shanghai response is not a result of selecting a temperature function that is more aggressive than MEGAN.

We have also revised the interpretation of the numerical attribution. The manuscript now states that, under the adopted isoprene-temperature parameterisation and Shanghai baseline emission setting, temperature-dependent isoprene accounts for approximately 70 % of the observed 30-40 °C O_3 increase (lines 846-850). This value quantifies the contribution within the controlled UKCA Box configuration; the central mechanistic result is that temperature-enhanced isoprene emissions provide a first-order amplification of O_3 under the VOC-limited Shanghai conditions. The direct JULES-MEGAN comparison shows that this mechanism remains strong under both formulations and is stronger, rather than weaker, when the MEGAN response is applied.

The revised manuscript also provides direct observational context for the simulated isoprene concentrations. Table 4 now compares the 30 °C baseline C_5H_8 concentrations with published observations from both environments. In Shanghai, the observed July daily mean is 0.8 μg m^{-3}, according to Gu et al. (2022), with a monthly averaged surface temperature of 29.3 °C (see https://tjj.sh.gov.cn/tjnj/nj19.htm?d1=2019tjnj/C0103.htm), whereas the simulated daily mean is 0.3 μg m^{-3}. The box model therefore does not produce excessive isoprene in the urban case; its concentration is lower than the available Shanghai observation. In Lishui, the observed

daytime mean is 8.3 μg m^{-3} with a temperature ranging from 28 to 35 ◦C (Geng et al., 2011) and the simulated daytime mean is 7.4 μg m^{-3}, showing close agreement in magnitude (Table 4; lines 501-510). These concentration comparisons directly constrain the chemical environments experienced by the model and support both the represented Shanghai-Lishui contrast and the magnitude of the baseline isoprene abundance.

We agree that anthropogenic VOC emissions can also respond to temperature, particularly through VCP-related solvent evaporation and gasoline evaporation. We have therefore added a targeted diagnostic calculation based on the temperature-dependent emission-scaling framework of Qin et al. (2025), using JJA 2022 CEDS emissions for Shanghai. Both source functions were normalised to the same 30 °C reference condition as the box-model experiments (Sect. 4.1; lines 777-784).

Between 30 and 40 °C, the selected VCP-related emission flux increases by 58.6 %, from 4.83 × 10^{-10} to 7.66 × 10^{-10} kg m^{-2} s^{-1}, while the gasoline-evaporation flux increases by 33.3 %, from 4.17 × 10^{-11} to 5.56 × 10^{-11} kg m^{-2} s^{-1}. The combined selected temperature-dependent AVOC flux consequently increases by 56.6 %, from 5.25 × 10^{-10} to 8.22 × 10^{-10} kg m^{-2} s^{-1} (lines 777-784). This demonstrates quantitatively that temperature-dependent AVOCs provide an additional urban VOC pathway during extreme heat.

The UKCA mechanism used in our study (StratTrop) contains only a limited subset of the alkanes, alkenes and aromatic compounds required to represent these evaporative sources explicitly. The AVOC calculation is therefore used to quantify the expected emission enhancement rather than to substitute an incomplete VOC mixture into the chemical mechanism. This distinction is now stated at lines 771-775. The revised Discussion also cites the Shanghai heatwave modelling of Qin et al. (2025), in which temperature-driven AVOC enhancements increased MDA8 O_3 by 4.6 ppb and peak O_3 by 7.5 ppb, demonstrating that the estimated AVOC response can produce an additional O_3 increase under hot urban conditions (lines 793-797).

We also examined whether the available evidence could identify whether temperature-dependent AVOC or BVOC emissions dominate the Shanghai VOC response. Within the present UKCA Box configuration, the explicitly represented temperature-dependent VOC response is necessarily dominated by isoprene because isoprene emissions respond directly to temperature, whereas the StratTrop mechanism represents only a limited subset of the relevant temperature-dependent urban AVOCs. The CEDS species retained by the current StratTrop emission mapping account for only 3.56 % of the selected gasoline-evaporation emissions and none of the selected VCP-related solvent emissions. Most of the temperature-dependent butanes, pentanes, higher alkanes, alkenes and aromatic compounds identified using the (Qin et al., 2025) framework are therefore absent from the explicit chemical sensitivity experiments.

The precursor-sensitivity diagnostics show that Shanghai remains strongly VOC-limited: O_3 increases with additional VOC availability and decreases with additional NO_x across 25-40 °C (Fig. 6a and 6c; lines 484-500). Baseline anthropogenic VOCs are therefore fundamental in establishing the urban chemical regime, temperature-dependent isoprene supplies the explicitly simulated biogenic amplification, and temperature-dependent evaporative AVOCs provide an additional anthropogenic enhancement during hot conditions.

Taken together, the revised evidence supports three conclusions. First, the JULES/iBVOC response is broadly consistent with MEGAN and is more conservative at the highest temperatures investigated. Second, available C_5H_8 observations do not indicate excessive simulated isoprene in Shanghai or Lishui. Third, temperature-dependent AVOCs can enhance urban precursor availability and O_3, but their inclusion does not remove the strong isoprene-driven mechanism diagnosed independently using both JULES and MEGAN. The revised manuscript now presents the BVOC percentage as configuration-specific while retaining the robust mechanistic conclusion that temperature-amplified isoprene emissions are an important driver of the Shanghai O_3 response.

Reviewer 1, Comment 5

Reviewer comment

5 There are concerns regarding the consistency between observations and model simulations at Lishui. The manuscript reports an underestimation of approximately 17 μg m^{-3} in daily mean ozone, while later sections indicate biases approaching 50 μg m^{-3} for daily maximum ozone. Such discrepancies are substantial and require a more rigorous explanation. The argument that these differences arise primarily from grid-scale dilution of precursor emissions appears insufficient, particularly given the relatively limited spatial scale represented by the model grid. Additional analysis is needed to explain the origin of these biases and assess their implications for the subsequent attribution results.

Response

We thank the reviewer for identifying the need to explain the Lishui comparison more precisely. We have revised the manuscript to distinguish explicitly between the local suburban environment sampled by the three Lishui AQMSs and the broader vegetation-rich, lower-NO_x rural environment that the Lishui box-model configuration was designed to represent. This distinction is now stated in Sect. 2.1 (lines 180-184), supported by the site and regional classifications in Table 1 and Fig. 1, and carried through the interpretation of the absolute O_3 comparison in Sect. 3.2 (lines 476-488) and Fig. 8 in Sect. 3.3 (lines 584-597). We have also clarified that the subsequent factorial attribution is based on relative O_3 changes within a fixed chemical environment rather than direct reproduction of station-level concentrations (lines 549-556 and 600-613; Table 5).

The reported differences of approximately 17 and 50 μg m^{-3} are not conflicting estimates of the same quantity. The 17 μg m^{-3} difference refers to daily mean O_3 in the 28.75-31.25 °C temperature bin: the simulated value is 35.8 μg m^{-3} and the observed value is 52.5 μg m^{-3} (lines 476-482). The approximately 50 μg m^{-3} difference refers to daily maximum O_3 across the binned O_3max-Tmax comparison in Fig. 8b (lines 584-591). Daily mean O_3 includes lower nighttime and morning concentrations, whereas daily maximum O_3 isolates the afternoon photochemical peak. A larger offset in O_3max is therefore consistent with the same underlying difference between the represented chemical environments.

The central point is that the Lishui box-model configuration was not designed to reproduce the immediate atmosphere surrounding the three monitoring stations. The AQMSs are located in the populated centre of Lishui and sample a local suburban receptor environment with a footprint of only several square kilometres. In contrast, the model was deliberately constructed to represent the more general vegetation-rich rural environment characteristic of the wider Lishui region. Its emissions were derived from regional inventory fields and its chemical baseline represents regional mean conditions with relatively low NO_x and stronger biogenic influence (Sect. 2.1, lines 180-184; Sect. 2.2.1, lines 250-304).

An exact like-for-like comparison is not possible because the available routine AQMS network does not include a station located in the broader forest-dominated rural environment represented by the box model, and the control sites and outside urban sites are not located in the targeted low-NO_x zone (their NOx levels are not in the lowest 25th percentile as a group; see Fig. 1b in R1C1). The three Lishui AQMSs are therefore used as the closest available observational reference. They are located within the same regional and climatic setting, occupy

the relatively low-NO_x end of the YRD monitoring distribution, and provide the available continuous local O_3 record for JJA 2022. We use these observations to assess whether the model reproduces the direction, shape and approximate magnitude of the O_3 response to temperature, rather than to validate the absolute O_3 concentration of the rural box-model environment. The remaining absolute offset is consistent with the difference between the populated urban/suburban receptor locations sampled by the AQMSs and the lower-NO_x, vegetation-rich regional environment represented by the model.

This is a purposeful distinction in the experimental design. The observational stations provide the available local O_3 record for evaluating the regional temperature response, while the box model represents the broader rural chemical environment required for the urban-rural mechanistic comparison. The revised manuscript therefore no longer attributes the difference simply to generic "grid-scale dilution". It identifies the two distinct receptor scales directly: a locally populated suburban monitoring environment and a regional, forest-dominated rural chemical environment.

The YRD-wide site analysis supports this interpretation. The three Lishui AQMSs have a mean JJA 2022 NO_2 concentration of 11.46 μg m^{-3}, around the 18th percentile of the 250-site YRD distribution, confirming that they sample a relatively low-NO_x part of the regional monitoring network. At the same time, two of the three stations lie within mapped urban-settlement polygons, demonstrating that they are not direct measurements of the surrounding rural landscape (Sect. 2.1, lines 148-161; Fig. 1 and Table 1). Lishui as a whole is much more strongly vegetated, with 81.7 % forest cover and an urban district occupying only approximately 8.6 % of its area (lines 158-161).

The new O_3-NO_x-isoprene response surface provides a chemical explanation for the direction of the offset. The Lishui baseline lies in a NO_x-limited regime: O_3 increases with additional NO_x and responds only weakly to additional isoprene (Fig. 6b and 6d; lines 484-500). The suburban monitoring sites are exposed to greater local anthropogenic NO_x influence than the regional rural box-model environment. Under NO_x-limited conditions, this greater local NO_x availability supports stronger afternoon O_3 production, producing higher observed O_3 at the monitoring sites than in the lower-NO_x regional box simulation.

The absolute offset does not undermine the subsequent process attribution because the attribution is not calculated from the difference between modelled and observed absolute O_3. It is derived from paired factorial experiments in which the same Lishui baseline environment is retained while temperature-dependent chemistry, humidity, the diurnal temperature cycle and isoprene-temperature coupling are switched on or off. The process contributions are therefore diagnosed from internally controlled changes between simulations (lines 600-613).

Table 3. Sensitivity experiments of the UKCA Box Model (VRH = fixed absolute humidity (=RH 70% at 30 °C); FRH = variable absolute humidity (=RH 70%))

Index	Experiment	RH	Diurnal cycle (D)	T-dependent isoprene emission (ft)	Environmental background
	Shanghai – Variable RH (VRH)				**Urban**
1	SH_VRH_Ori	Change with T	No	No	Urban
2	SH_VRH_D	Change with T	Yes	No	Urban

3	SH_VRH_ft	Change with T	No	Yes	Urban
4	SH_VRH_Dft	Change with T	Yes	Yes	Urban
	Lishui – Variable RH (VRH)				**Rural**
5	LS_VRH_Ori	Change with T	No	No	Rural
6	LS_VRH_D	Change with T	Yes	No	Rural
7	LS_VRH_ft	Change with T	No	Yes	Rural
8	LS_VRH_Dft	Change with T	Yes	Yes	Rural
	Shanghai – Fixed RH (RH = 70%)				**Urban**
9	SH_FRH_Ori	Fixed at 70%	No	No	Urban
10	SH_FRH_D	Fixed at 70%	Yes	No	Urban
11	SH_FRH_ft	Fixed at 70%	No	Yes	Urban
12	SH_FRH_Dft	Fixed at 70%	Yes	Yes	Urban
	Lishui – Fixed RH (RH = 70%)				**Rural**
13	LS_FRH_Ori	Fixed at 70%	No	No	Rural
14	LS_FRH_D	Fixed at 70%	Yes	No	Rural
15	LS_FRH_ft	Fixed at 70%	No	Yes	Rural
16	LS_FRH_Dft	Fixed at 70%	Yes	Yes	Rural

Importantly, the model reproduces the magnitude of the observed temperature-driven increase despite its lower absolute baseline. Between 30 and 40 °C, observed Lishui O_3max increases by 26.21 μg m^{-3}. The corresponding increases are 21.08 μg m^{-3} in VRH_Ori (experiment settings see the Table 3 above), 22.40 μg m^{-3} in VRH_D, 23.81 μg m^{-3} in VRH_ft and 21.57 μg m^{-3} in VRH_Dft (Table 5). The simulations therefore capture the observed approximately 21-26 μg m^{-3} warming response and reproduce the shape of the observed O_3-temperature relationship, while remaining systematically lower in absolute concentration (Fig. 8b; lines 584-597).

The manuscript consequently interprets the Lishui experiments as a diagnosis of the relative temperature sensitivity of a representative vegetation-rich rural chemical environment, rather than as a direct simulation of the suburban monitoring stations. The consistent O_3-temperature response, the independently diagnosed NO_x-limited regime and the internally controlled factorial design provide a robust basis for the Lishui attribution results despite the expected difference in absolute O_3 between the local observations and the broader rural model environment.

Reviewer 1, Comment 6

Reviewer comment

6 The manuscript uses UKESM diagnostics to evaluate the chemical performance of the box model, yet little information is provided regarding the performance of UKESM itself over the YRD region. Since UKESM operates at relatively coarse spatial resolution, its ability to reproduce local ozone variability and ozone-temperature relationships should be evaluated before it is used as a benchmark for the box-model analysis. In addition, the manuscript attributes differences in O_x sink terms between the box model and UKESM to unresolved transport processes in the box model. However, no explicit diagnostics of horizontal transport, vertical mixing, or other dynamical terms are presented from UKESM. Providing these diagnostics would greatly strengthen the interpretation.

Response

We thank the reviewer for identifying the need to clarify the role of UKESM-AMIP in the analysis. We have revised the manuscript throughout to remove the previous implication that UKESM is used as a benchmark or formal evaluation standard for the UKCA Box model. The Methods now define the UKCA Box model as the primary controlled process-attribution framework and UKESM-AMIP as a supporting three-dimensional simulation using the same StratTrop chemical mechanism (Sect. 2.2.1, lines 209-231; Sect. 2.2.2, lines 309-330). Section 3.2 now states explicitly that the purpose is not to evaluate the box model formally against UKESM or observations (lines 463-468). Figure 7 and its discussion have also been reframed as a comparison of selected fractional O_x pathways rather than a validation of local O_3 concentrations or O_3-temperature variability (lines 514-548), and the interpretation of the subsequent experiments is now based on relative process sensitivity and chemical-regime behaviour (lines 549-556).

The reviewer requested an evaluation of UKESM's local O_3 variability, which would be essential if UKESM were being used as an observational benchmark. This is not the role assigned to UKESM in the revised manuscript. The controlled temperature-attribution experiments are performed with the UKCA Box model, while UKESM-AMIP is used only to provide a three-dimensional chemical context for selected O_x production and loss pathways. We therefore do not use UKESM to establish whether the box model reproduces station-level O_3 concentrations, daily variability, or the observed O_3-temperature slopes.

The value of this comparison is that the two frameworks use the same StratTrop gas-phase chemical mechanism but differ fundamentally in their physical representation. The UKCA Box model isolates local chemical responses to prescribed temperature, humidity and precursor conditions without advection, convection or diffusion. UKESM-AMIP represents the same chemistry within a three-dimensional atmosphere containing transport, boundary-layer mixing, convection and meteorological variability (lines 209-231 and 309-330). Comparing their fractional chemical budgets (Figure 7) therefore tests whether the dominant chemical pathways identified in the controlled box environment are also present in a three-dimensional same-chemistry simulation.

Unfortunately, the currently available UKESM diagnostics do not provide a separate quantitative decomposition of horizontal advection, vertical entrainment, convection and ventilation, and it is not a simple task to add these diagnostics. The interpretation therefore

does not assign the difference in Fig. 7 to any individual dynamical pathway. It identifies only the aggregate effect of physical exchange that is represented in the three-dimensional model but absent from the closed box model.

In the UKCA Box model, the air parcel is closed and well mixed, and all non-chemical removal absent from the model must be represented through the parameterised lower-boundary loss. In UKESM-AMIP, physical exchange redistributes and exports O_x through the resolved three-dimensional circulation. The UKESM residual shown in Figure 7 therefore represents the aggregate contribution required to close the O_x budget after the diagnosed chemical production, chemical loss and deposition terms are considered; it is not presented as an explicit diagnostic of any individual transport process. This distinction is now stated directly at lines 537-548, and the Figure 7 caption identifies the box-model green term as dry deposition plus effective physical-export loss (lines 514-520).

The larger fractional lower-boundary loss in the box model should therefore not be interpreted as evidence that true surface deposition is physically stronger than in UKESM. It reflects the structural requirement that chemical production in a closed, steady-state box must be balanced without the transport and ventilation pathways available in the three-dimensional simulation. The comparison consequently illustrates the effect of including versus excluding physical exchange, while avoiding unsupported attribution among individual dynamical terms.

The UKESM comparison is also only one component of the chemical assessment in Sect. 3.2. The revised section combines three complementary diagnostics: the O_3-NO_x-isoprene response surfaces, contextual comparison of selected chemical species with observations, and comparison of the dominant O_x pathways with the same-chemistry UKESM-AMIP simulation (lines 463-468). Together, these diagnostics establish the contrasting VOC-limited Shanghai-like and NO_x-limited Lishui-like environments and support use of the box model as a method for investigating the roles of chemical processes.

Accordingly, the revised manuscript no longer treats UKESM-AMIP as a benchmark for local YRD O_3 behaviour. Its role is restricted to demonstrating whether the dominant O_x chemical pathways diagnosed in the box model are structurally consistent with those produced by the same chemistry in a three-dimensional atmosphere. The revised interpretation also makes clear that Figure 7 does not quantify individual transport or mixing contributions. This narrower and more precise use of UKESM directly addresses the reviewer's concern while preserving the scientifically useful same-chemistry comparison.

Reviewer 1, Comment 7

Reviewer comment

7 The attribution framework appears to place primary emphasis on chemical processes, including temperature-dependent reaction kinetics, BVOC emissions, and humidity effects, while giving relatively limited consideration to other processes that co-vary with temperature. Previous studies have shown that ozone-temperature relationships can also be strongly influenced by changes in solar radiation, cloud cover, atmospheric stagnation, boundary-layer dynamics, transport processes, and temperature-sensitive natural emissions (e.g., soil NO_x)(Fu and Tian, 2019; Lu et al., 2019). Several recent studies have further demonstrated that the ozone climate penalty arises from the combined effects of chemical and meteorological drivers rather than from chemistry alone(Barnes and Fiore, 2013; Kerr et al., 2020; Porter and Heald, 2019).

This issue is particularly important because the attribution results presented in Lines 566-570 suggest that deposition and transport play only a minor role in the ozone response to temperature. Such a conclusion appears difficult to reconcile with a number of previous studies that identified meteorological covariability and transport-related processes as major contributors to ozone-temperature sensitivity. The authors should therefore provide a more comprehensive discussion of how their attribution framework differs from those used in previous studies and explain why their results yield substantially different relative contributions.

Barnes, E. A. and Fiore, A. M.: Surface ozone variability and the jet position: Implications for projecting future air quality, Geophys. Res. Lett., 40, 2839-2844, https://doi.org/10.1002/grl.50411, 2013.

Fu, T.-M. and Tian, H.: Climate Change Penalty to Ozone Air Quality: Review of Current Understandings and Knowledge Gaps, Curr. Pollut. Rep., 5, 159-171, https://doi.org/10.1007/s40726-019-00115-6, 2019.

Kerr, G. H., Waugh, D. W., Steenrod, S. D., Strode, S. A., and Strahan, S. E.: Surface Ozone-Meteorology Relationships: Spatial Variations and the Role of the Jet Stream, J. Geophys. Res. Atmospheres, 125, e2020JD032735, https://doi.org/10.1029/2020JD032735, 2020.

Lu, X., Zhang, L., and Shen, L.: Meteorology and Climate Influences on Tropospheric Ozone: a Review of Natural Sources, Chemistry, and Transport Patterns, Curr. Pollut. Rep., 5, 238-260, https://doi.org/10.1007/s40726-019-00118-3, 2019.

Porter, W. C. and Heald, C. L.: The mechanisms and meteorological drivers of the summertime ozone-temperature relationship, Atmospheric Chem. Phys., 19, 13367-13381, https://doi.org/10.5194/acp-19-13367-2019, 2019.

Response

We thank the reviewer for this important comment and for drawing our attention to these relevant publications. We agree that the complete atmospheric O_3-temperature relationship is influenced by meteorological and physical processes in addition to chemistry and precursor emissions. These publications provide valuable guidance for our planned follow-up study,

which will investigate the meteorological contribution to summertime O_3 variability using a three-dimensional modelling framework.

The purpose of the present study, however, is specifically to isolate the chemical temperature response and selected temperature-dependent emission effects under controlled environmental conditions. We have revised the manuscript to make this scope considerably clearer. The Introduction now describes the broader roles of emissions, chemistry, transport and deposition in linking temperature to surface O_3 (lines 43-102), and then states explicitly that the present attribution study focuses on processes that can be isolated within the UKCA Box model (lines 115-126). The Methods further clarify that the sensitivity experiments quantify local chemical and emission-related responses to prescribed temperature and humidity, rather than providing a complete decomposition of all meteorological controls on the observed O_3-temperature relationship (lines 375-385). The Conclusions now repeat this scope and identify meteorological attribution as a priority for subsequent work (lines 893-908).

The UKCA Box model is designed to separate the effects of temperature-dependent gas-phase chemistry, humidity-related chemistry, diurnal temperature structure and isoprene emissions. Three-dimensional processes such as changing solar radiation associated with clouds, atmospheric stagnation, horizontal transport, boundary-layer development, entrainment, convection and precipitation cannot easily be varied or diagnosed independently within this framework. Assigning quantitative contributions to these processes would require a regional or global three-dimensional model with dedicated meteorological and transport diagnostics, which is outside the scientific target of the present analysis.

The reported process fractions are explicitly defined as the chemical and selected emission-related contributions resolved by the controlled box-model experiments, rather than a complete attribution of the observed O_3-temperature relationship. The manuscript likewise does not conclude that transport and deposition are generally minor controls on atmospheric O_3. These physical processes are not assigned independent temperature-response fractions because they are not separately perturbed within the experimental design.

The revised manuscript consequently distinguishes the present chemical attribution from the broader meteorological attribution frameworks used in the studies cited by the reviewer. Those studies investigate the combined influence of meteorology, circulation, transport, emissions and chemistry, whereas our experiments isolate the chemical response to prescribed temperature and humidity under contrasting precursor regimes. The approaches therefore address complementary scientific questions rather than producing directly comparable process fractions.

We have made this distinction explicit throughout the revised manuscript. The current study establishes the chemical mechanisms responsible for contrasting O_3 temperature responses in Shanghai and Lishui, while the meteorological and physical contributions, including transport, boundary-layer dynamics, stagnation, clouds and radiation, will form the focus of our following three-dimensional modelling study.

Reviewer 1, Other Comment 1

Reviewer comment

1 Lines 182-183: Why were the years 2020 and 2021 excluded? Does this exclusion have any impact on the selection of heatwave days?

Response

We thank the reviewer for this question. We have clarified the reference-period selection and its effect on the heatwave classification in Sect. 2.1 (lines 185-192).

The years 2020 and 2021 were excluded so that the heatwave threshold was calculated from a consistent pre-COVID reference climatology, avoiding the exceptional activity and emission conditions associated with the pandemic period. Heatwave days are identified exclusively from daily maximum temperature relative to the smoothed 90th-percentile threshold; air-pollution concentrations and emissions are not used in this classification.

The exclusion of 2020-2021 therefore does not remove or alter any of the 2022 heatwave days. These years are excluded only from the reference-period calculation used to define the meteorological threshold.

Reviewer 1, Other Comment 2

Reviewer comment

2 Line 217: Why did the authors choose to use the CEDS inventory instead of the MEIC inventory?

Response

We thank the reviewer for this question. We have clarified the choice of anthropogenic emission inventory in Sect. 2.2.1 (lines 260-269).

We appreciate that MEIC provides a more locally specific representation of anthropogenic emissions over China. CEDS was selected because it is widely used in chemistry-climate modelling and is also the anthropogenic inventory applied in the UKESM-AMIP simulation. Using CEDS in the UKCA Box model therefore maintains consistency between the two modelling frameworks and avoids introducing an additional difference caused solely by using separate emission inventories.

Reviewer 1, Other Comment 3

Reviewer comment

3 Line 287: 30C to 30°C

Response

We thank the reviewer for identifying this formatting issue. We have corrected “30C” to “30 °C” and checked the manuscript to ensure that temperatures are presented consistently using the same format throughout.

Reviewer 1, Other Comment 4

Reviewer comment

4 Line 326: Why was 38.3 chosen as the stagnation point?

Response

We thank the reviewer for this question. The value of 38.3 °C follows directly from the adopted JULES isoprene temperature-response function (Pacifico et al., 2011): fT = min[exp(0.1(T - 30)), 2.3].

The emission multiplier reaches its prescribed upper limit of 2.3 at 38.3 °C and therefore remains constant above this temperature.

Reviewer 1, Other Comment 5

Reviewer comment

5 Figure 4: Is this the average result across all sites? How was the spatial variability of ozone concentrations among different sites accounted for?

Response

We thank the reviewer for this question. We have clarified the data aggregation in Sect. 2.1 (lines 172-177) and the Figure 4 caption (lines 388-392).

Figure 4 presents site-averaged results. Hourly O_3 concentrations were first averaged across the eight retained Shanghai sites and, separately, across the three retained Lishui sites. Daily maximum O_3 was then calculated from each aggregated hourly series.

All retained sites therefore contribute equally to the corresponding city-level relationship, reducing the influence of individual-site anomalies. The locations and environmental settings of the individual monitoring sites are shown in Figure 1 and Table 1. Figure 4 is intended to represent the common Shanghai and Lishui signals rather than station-specific regressions.

References

Archer-Nicholls, S., Abraham, N. L., Shin, Y. M., Weber, J., Russo, M. R., Lowe, D., Utembe, S. R., O'Connor, F. M., Kerridge, B., Latter, B., Siddans, R., Jenkin, M., Wild, O., and Archibald, A. T.: The Common Representative Intermediates Mechanism Version 2 in the United Kingdom Chemistry and Aerosols Model, Journal of Advances in Modeling Earth Systems, 13, e2020MS002420, https://doi.org/10.1029/2020MS002420, 2021.
Cheng, X., Li, H., Zhang, Y., Li, Y., Zhang, W., Wang, X., Bi, F., Zhang, H., Gao, J., Chai, F., Lun, X., Chen, Y., Gao, J., and Lv, J.: Atmospheric isoprene and monoterpenes in a typical urban area of Beijing: Pollution characterization, chemical reactivity and source identification, Journal of Environmental Sciences, 71, 150-167, https://doi.org/10.1016/j.jes.2017.12.017, 2018.
Geng, F., Tie, X., Guenther, A., Li, G., Cao, J., and Harley, P.: Effect of isoprene emissions from major forests on ozone formation in the city of Shanghai, China, Atmos. Chem. Phys., 11, 10449-10459, 10.5194/acp-11-10449-2011, 2011.
Gu, C., Wang, S., Zhu, J., Wu, S., Duan, Y., Gao, S., and Zhou, B.: Investigation on the urban ambient isoprene and its oxidation processes, Atmospheric Environment, 270, 118870, https://doi.org/10.1016/j.atmosenv.2021.118870, 2022.
Guenther, A. B., Jiang, X., Heald, C. L., Sakulyanontvittaya, T., Duhl, T., Emmons, L. K., and Wang, X.: The Model of Emissions of Gases and Aerosols from Nature version 2.1 (MEGAN2.1): an extended and updated framework for modeling biogenic emissions, Geosci. Model Dev., 5, 1471-1492, 10.5194/gmd-5-1471-2012, 2012.
Min, K. E., Pusede, S. E., Browne, E. C., LaFranchi, B. W., and Cohen, R. C.: Eddy covariance fluxes and vertical concentration gradient measurements of NO and NO₂ over a ponderosa pine ecosystem: observational evidence for within-canopy chemical removal of NO_x, Atmos. Chem. Phys., 14, 5495-5512, 10.5194/acp-14-5495-2014, 2014.
Pacifico, F., Harrison, S. P., Jones, C. D., Arneth, A., Sitch, S., Weedon, G. P., Barkley, M. P., Palmer, P. I., Serça, D., Potosnak, M., Fu, T. M., Goldstein, A., Bai, J., and Schurgers, G.: Evaluation of a photosynthesis-based biogenic isoprene emission scheme in JULES and simulation of isoprene emissions under present-day climate conditions, Atmos. Chem. Phys., 11, 4371-4389, 10.5194/acp-11-4371-2011, 2011.
Qin, M., She, Y., Wang, M., Wang, H., Chang, Y., Tan, Z., An, J., Huang, J., Yuan, Z., Lu, J., Wang, Q., Liu, C., Liu, Z., Xie, X., Li, J., Liao, H., Pye, H. O. T., Huang, C., Guo, S., Hu, M., Zhang, Y., Jacob, D. J., and Hu, J.: Increased urban ozone in heatwaves due to temperature-induced emissions of anthropogenic volatile organic compounds, Nature Geoscience, 18, 50-56, 10.1038/s41561-024-01608-w, 2025.
Wesely, M. L.: Parameterization of surface resistances to gaseous dry deposition in regional-scale numerical models, Atmospheric Environment (1967), 23, 1293-1304, https://doi.org/10.1016/0004-6981(89)90153-4, 1989.
Wu, K., Yang, X., Chen, D., Gu, S., Lu, Y., Jiang, Q., Wang, K., Ou, Y., Qian, Y., Shao, P., and Lu, S.: Estimation of biogenic VOC emissions and their corresponding impact on ozone and secondary organic aerosol formation in China, Atmospheric Research, 231, 104656, https://doi.org/10.1016/j.atmosres.2019.104656, 2020.
Yin, Q., Ma, Q., Lin, W., Xu, X., and Yao, J.: Measurement report: Long-term variations in surface NOx and SO2 mixing ratios from 2006 to 2016 at a background site in the Yangtze River Delta region, China, Atmos. Chem. Phys., 22, 1015-1033, 10.5194/acp-22-1015-2022, 2022.